Research Article

Journal of Molecular Recognition

Received: 1 November 2011, Revised: 14 March 2012, Accepted: 15 March 2012, Published online in Wiley Online Library

(wileyonlinelibrary.com) DOI: 10.1002/jmr.2187

# Software for drift compensation, particle tracking and particle analysis of high-speed atomic force microscopy image series†

Mohamed Husain[a], Thomas Boudier[b], Perrine Paul-Gilloteaux[c], Ignacio Casuso[a] and Simon Scheuring[a]*

**Atomic force microscopy (AFM) image acquisition is performed by raster-scanning a faint tip with respect to the sample by the use of a piezoelectric stage that is guided by a feedback system. This process implies that the resulting images feature particularities that distinguish them from images acquired by other techniques, such as the drift of the piezoelectric elements, the unequal image contrast along the fast- and the slow-scan axes, the physical contact between the tip of nondefinable geometry and the sample, and the feedback parameters. Recently, high-speed AFM (HS-AFM) has been introduced, which allows image acquisition about three orders of magnitude faster (500–100 ms frame rate) than conventional AFM (500 s to 100 s frame rate). HS-AFM produces image sequences, large data sets, which report biological sample dynamics. To analyze these movies, we have developed a software package that (i) adjusts individual scan lines and images to a common contrast and *z*-scale, (ii) filters specifically those scan lines where increased or insufficient force was applied, (iii) corrects for piezo-scanner drift, (iv) defines particle localization and angular orientation, and (v) performs particle tracking to analyze the lateral and rotation displacement of single molecules. Copyright © 2012 John Wiley & Sons, Ltd.**

**Keywords:** high-speed AFM; analysis software

## INTRODUCTION

Atomic force microscopy (AFM; Binnig *et al*., 1986) is a powerful tool for the characterization of biological molecules. It acquires high-resolution topographic data of the biological molecules in physiological buffer and at ambient temperature and pressure (Schabert *et al*., 1995). In particular, AFM has been extensively used for obtaining the surface structures of proteins (Engel and Gaub, 2008) and for force measurements (Rico *et al*., 2005; Rief *et al*., 1997), making AFM a complementary technique to X-ray crystallography, nuclear magnetic resonance, and electron microscopy (Parot *et al*., 2007). With recent technical improvements, it is possible to scan at a higher speed (Fantner *et al*., 2006; Viani *et al*., 2000; Viani *et al*., 1999). In particular, the acquisition rate (time per frame) of a biology-adapted high-speed AFM (HS-AFM) has been reduced by about three orders of magnitude (100 ms per frame) (Ando *et al*., 2001). Using this technology, it is now possible to visualize the biochemical processes in action by providing concrete visual evidence of the structure–function relation and hence an in-depth understanding of the molecules in their native state (Kodera *et al*., 2010).

Generally, AFM images and HS-AFM image sequences contain various particularities because of the scanning process (VanCleef *et al*., 1996). The images are the super position of signal and noise (Unser *et al*., 1987). In AFM, the signal emerges from contouring the object whereas the noise originates from the apparatus or is acquisition related (Fechner *et al*., 2009). It has been shown that the noise in the images can be assessed using the cross-correlation value (CCV) of an imaged protein compared with a noise-free or artificial reference or its internal symmetry (IS) (Fechner *et al*., 2009).

During the process of single molecule observation in HS-AFM experiments, the surface-contouring precision of the fast feedback loop is slightly varying probably because of the minor force drift, that is, the absolute distance in *z*-dimension between tip and sample stage. Because of the high acquisition frame rate and the slowness of the human operator reaction for force readjustment, not all images are of equal quality. Indeed, in the final movie, highly contrasted images may alternate when forces were well adjusted and frames were acquired with variant imaging forces resulting in low-contrast contouring of the molecules. Force drift may be caused by noncontrollable physical phenomena like dilation, surface tension variations, laser fluctuations, temperature drift or electrical changes, and so on (Casuso and Scheuring, 2010). Although the drift can be detected and >monitored, it is very difficult to eliminate drift in AFM and HS-AFM systems (Ando *et al*., 2008). The

* *Correspondence to: Simon Scheuring, U1006 INSERM, Université Aix-Marseille, Parc Scientifique de Luminy, Marseille F-13009, France. E-mail: simon.scheuring@inserm.fr*

† *This article is published as part of the AFM BioMed Conference on Life Sciences and Medicine, Paris 2011 of the Journal of Molecular Recognition, edited by Simon Scheuring, Pierre Parot and Jean-Luc Pellequer.*

a *M. Husain, I. Casuso, S. Scheuring*
*U1006 INSERM, Université Aix-Marseille, Parc Scientifique de Luminy, Marseille, F-13009, France*

b *T. Boudier*
*Université Pierre et Marie Curie, 7 Quai St Bernard, Paris, F-75252, France*

c *P. Paul-Gilloteaux*
*Institut Curie, Pict-IBISA, UMR144 CNRS, 26 rue, d'Ulm, Paris, F-75248, France*

problem of force drift can be tackled physically to some extend (Casuso and Scheuring, 2010; de Pablo *et al*., 1998; Kindt *et al*., 2002); however, thorough image analysis and subsequent specific filtering significantly improve the visualization of biomolecular processes (Chen and Pellequer, 2011; van Noort *et al*., 1999).

In addition to force drift in *z*-dimension, the scanner stage can also drift by some nanometers in *x*- and *y*-dimension, especially during the seconds after execution of a position or scan range change due to piezo-relaxation (Thomson *et al*., 1996). Tackling this problem is more challenging for HS-AFM than for conventional AFM because HS-AFM objects are observed, which are dynamic and change molecular arrangement with time (Casuso *et al*., 2010; Kodera *et al*., 2010). Again, thorough image analysis allows the alignment of movie frames either by aligning subsequent frames by their overall resemblance or by aligning stable significant features.

Aligned movie frames can then be analyzed, defining for each molecule the degrees of freedom, the position ($x$, $y$), and the rotation angle ($\alpha$) in each frame recorded at time ($t$), in analogy to cross-correlation-based image treatment of conventional AFM (Fechner *et al*., 2009; Schabert and Engel, 1994). The derived data can be used for particle tracking, in analogy to fluorescence molecule tracking using optical microscopy (Kusumi *et al*., 1993), with the significant advantages of higher resolution, the observation of unlabelled proteins, and the concomitant observation of the molecular environment (Casuso *et al*., 2010).

Every imaging technique needs image analysis tools that are adapted to their qualities, specificities, and shortcomings. In this work, we present the rationales and developments of a movie analysis software package dedicated to HS-AFM, an emerging young technique that is proving at the moment its power to unravel previously inaccessible dynamic biological phenomena (Casuso *et al*., 2012; Casuso *et al*., 2010; Kodera *et al*., 2010; Shibata *et al*., 2010).

## MATERIALS AND METHODS

### High-speed atomic force microscopy

A high-speed atomic force microscopy (HS-AFM) (Ando *et al*., 2001) equipped with 8-μm-long cantilevers (spring constant $k = 0.2$ N/m, resonance frequency $f_{(r)} = 700$ kHz; NanoWorld, Neuchâtel, Switzerland) featuring an electron beam deposition tip was used for image acquisition. The images analyzed in this work were acquired in oscillating mode, exciting the cantilever at resonance frequency, at a scan rate of 477 ms/frame, a scan size of 75 nm, and a *z*-range of 4 nm (Casuso *et al*., 2012), except for the image shown in Figure 2B, which is acquired at a scan rate of 1000 ms/frame, a scan size of 15 nm, and a *z*-range of 0.5 nm.

### Data analysis

The HS-AFM image analysis and the treatment package presented in this work are JAVA-based image processing routines integrated in the ImageJ image analysis platform (Rasband, 1997–2011). The images analyzed in this work had an image size of 300 × 300 pixels and were 8-bit gray-scale formatted.

## RESULTS

### Line-by-line contrast adjustment and noise reduction

During single molecule observation in HS-AFM experiments, the surface-contouring precision of the fast feedback loop is slightly varying, probably due to minimal force drift. In the final resulting images, well-adjusted and insufficient imaging force is represented by high- and low-contrast contouring of the molecules. In the first step, our aim is to adjust image contrast because improved contrast will aid any further data treatment and visibility. However, in AFM, the notion of an "image" does not make that much sense because the first scan line of a frame is timewise more related to the last scan line of the frame before than to scan lines within its image frame; briefly, the scan line is the minimal information unit that must be treated. To do so, we must first know the characteristics of a good scan line. For this, it is straightforward to have a close look at the histogram statistics of good scan lines. A hand-selected well-contrasted image frame contains 300 scan lines (Figure 1A); from these, we extract line by line the minimum value (Figure 1B, first panel), the maximum value (Figure 1B, second panel), the average value (Figure 1B, third panel), and the standard deviation of the gray value distribution in each line (Figure 1B, fourth panel). These four characteristics will be used by the program to distinguish automatically good from bad individual scan lines. For example, if a scan line has been acquired at insufficient applied force, the tip does not penetrate between molecules, and the minimum value will deviate from the one found in good scan lines; on the other hand, maximum values may deviate when the applied force was too high and molecules are squeezed and the average and standard deviation values deviate in noisy scan lines, that is, the gray value distribution is dominated by the noise what leads the average value to be noise centered, and the standard deviation value to diminish. The program uses "if loops" for each criterion, for example, *if (minavg* $<$ *avg) && (avg* $<$ *maxavg)*, where *minavg* is the minimal average value of the 300 scan lines in the best frame, *maxavg* is the maximum average value of the 300 scan lines in the best frame, and *avg* is the average value of the line that is being tested. Contrast change may arise between frames or between lines within one image, such as a frame where the top half of the image is well contrasted while the bottom half exposes lower contrast (Figure 1C). Our interpretation is that the molecular topography is accurately contoured when the force is optimal (Figure 1C, top half), but the tip is not going sufficiently down in between molecules when the scanning force is insufficient (Figure 1C, bottom half). This force drift may emerge from mechanical and thermal drifts and from charging effects that alter the effective tip-sample distance. Using one, several, or all of the above-described criteria (see panels in Figure 1B), a list is generated that inventories the bad scan lines (Figure 1D), those that do not satisfy the reference values used as criteria. As can be seen, for the particular frame 104 (Figure 1C), only few bad lines are found in the top part of the image (lines 66, 67, 68, 69, 71, and 72), but many bad lines are found from about the middle of the image downwards (lines 127, 128, 130, 131, etc.) (Figure 1D), in agreement with visual inspection. Those lines identified as bad lines are subsequently filtered using a median filter (with adjustable width of 1, 2, or 3 pixels) (Figure 1E) and contrast adjusted (Figure 1F). Because contrast changes can appear within an individual image frame, we could not adjust contrast on images but needed to adjust the contrast line by line, in a manner that expands the histogram to identical minimum and maximum values per scan line (Figure 1F). This treatment is clearly justified, as we observe identical transmembrane molecules within one membrane, given that the molecules protrude by the same height and the membrane is flat within the measurement error. The beneficial effect of the entire procedure is nicely illustrated in line profiles (Figure 1G), and although the



  

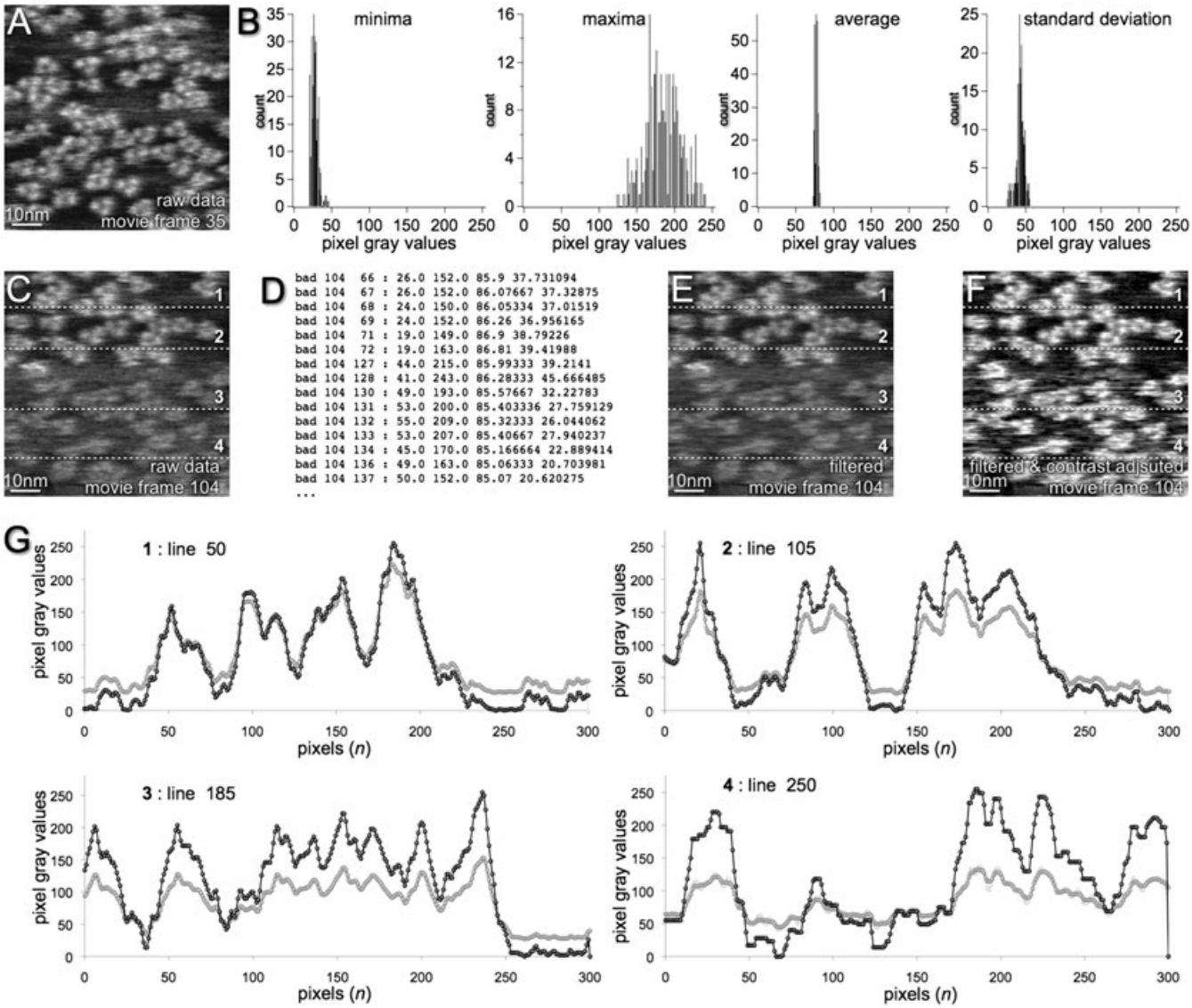


**Figure 1**. Contrast enhancement and noise reduction of HS-AFM movies. (A) Highly contrasted raw data image frame (full image size, 750Å; full gray scale 40Å). (B) Histograms of the 300 scan lines in panel A. Plots (from left to right): minima, maxima, average, and standard deviation values. (C) Raw data image frame containing a highly contrasted (top) and a low-contrasted region (bottom). (D) Part of the list of bad lines in frame shown in panel C. (E) Filtered and (F) line-by-line contrast-enhanced panel C. (G) Profile analyses of scan lines 50, 105, 185, and 250 (outlined in C, E, and F) before (gray line) and after filtering and contrast enhancement (black line).

effect is less significant in the highly contrasted sections 1 and 2 (lines 50 and 105 in images C, E, and F; Figure 1G, top), the benefit is obvious in traces from the low-contrasted region, sections 3 and 4 (lines 185 and 250 in images C, E and F; Figure 1G, bottom). Indeed, the initial histogram of the highly contrasted lines ranged from ~30 to ~200, whereas the low-contrast traces ranged from ~40 to ~125 gray values (full initial gray scale 0 to 255 is 40Å). After line-by-line histogram leveling, the full gray value range is reset to 27Å but equal in all lines of all frames. Obviously, contrast adjustment alone also boosts the noise in low-contrasted traces. Indeed, insufficient imaging force has as consequences not only lower contrast but also increased noise, probably because the lever vibrates more when forces are low. That is why we first perform a median filter and then readjust the contrast on the individual bad lines. Taken together, we adjust each scan line contrast individually and de-noise only those that do not suffice criteria for good lines. As a result, some lines, the badly contoured ones, will have lower resolution, but the visibility of the molecular movements is significantly improved. This entire process is computationally fast and takes just fractions of seconds on a conventional personal computer for treating some tens of thousands of scan lines.

### HS-AFM movie "stabilization"—piezo-scanner drift correction

Before any data can be extracted from HS-AFM image sequences, all images must be perfectly aligned with respect to a stable coordinate origin. Indeed, mechanical drift of the HS-AFM setup and piezo-scanner creep may result into movies in which the sequential frames are not perfect real-space superpositions. The major source of drift originates from the piezo-elements in the scanner. When a voltage is applied to a piezoelectric element, it expands or retracts to attain the corresponding position. However, this process is not instantaneous

and not without error. Typically, a piezo to which a voltage change is applied first "overshoots," that is, goes beyond the expected position, and second relaxes to a stable position. Five frames taken within the first 3816 ms after scan positioning of movie acquisition are shown (Figure 2A), in which an assembly of proteins and their environment can be observed (outline in Figure 2A), drifting from the left to the right and slightly from the top to the bottom. Once the scanner piezos are kept for a longer period at constant voltage, they are very precise and stable, allowing the imaging of the atomic lattice on mica surfaces (Figure 2B).

To analyze correctly the molecular positions of the proteins, we first have to compensate for drift (Figure 2A). Particularly challenging as we observe objects that are themselves dynamic is that the three porin trimers outlined change their molecular arrangement with time.

However, biological samples are fragile, and scanning the same area over very long experimental periods is critical. Therefore, piezo scanner drift can be a problem for biological HS-AFM image acquisition. Other minor effects, like mechanical or thermal drift, might contribute to unstable image position preservation in subsequent frames. However, we feel these effects are minor, and it is anyway largely impossible to distinguish and isolate the contributions of these different effects. All that can be performed is designing a most stable AFM setup and uncouple it from the environment as well as possible. Finally, it is the result, the HS-AFM movie itself, that reports about the total drift present during acquisition, within which each individual movie frame must be aligned to a novel corrected origin to generate a drift-corrected "stabilized" movie.

Of course, it is of highest importance to note from the beginning that we want to stabilize subsequent frames from drift, although we expect them to contain moving parts, that is, molecules. It is possible and justified to compensate for drift, despite molecular movements in the frames, because molecular movements are random and fast whereas drift is directed and slow. The process of movie drift correction is illustrated in Figure 3. A raw data movie is a series of frames with dimensions *XY*, stacked as a function of frame acquisition time *T*. We term these movies *XYT* stacks (Figure 3A, individual *XY* frame 36). The calculation of a kymograph, an *XTY* stack, an image sequence in which every frame contains the "same" scan line acquired over the entire movie acquisition period, nicely illustrates the drift problem. The molecules contoured in line 75, for example, are expected to be relatively stable as long as they are present at their relative *XY* position, whereas those that move across line 75 appear and disappear as a few bright pixels in a kymograph. In frame 75 of the *XTY* kymograph of the original movie, topography features are represented by arcs (Figure 3B, individual XT frame containing all lines 75). Obviously, the position changed for all molecules in the same direction and at the same speed, a clear indication that the overall *XY* coordinate origin has not been kept fixed during movie acquisition. In a two-step process, we establish a movie drift correction coordinate list. This list contains for each image frame (*n*) a pixel compensation value in *X*- and *Y*-direction that will shift the origin of each frame by values *X* and *Y* to a novel origin (Figure 3C). To obtain this list, we first perform a manual origin alignment by defining on each frame a coordinate that is the novel origin; usually, a particularly well-recognizable and stable topography feature or molecular constellation is chosen. The resulting drift correction coordinate list can be used to create a "rough aligned movie" (Figure 3C, traces labeled "rough align"). This step can be omitted in case that the overall drift in the movie is minor. In case that it is necessary, it takes approximately 1 s per frame to define with the cursor a novel rough origin. Second, an image area (or the entire image) in frame 1 of the "rough aligned movie" is chosen as reference for aligning frame 2 to frame 1 using automatic cross correlation, following

$$\mathrm{CCV} = \frac{\sum_i \left(R_{(i)} - \bar{R}\right) \times \left(F_{(i)} - \bar{F}\right)}{\sqrt{\sum_i \left(R_{(i)} - \bar{R}\right)^2 \times \left(F_{(i)} - \bar{F}\right)^2}}$$

where each pixel (*i*) in the reference (*R*) is compared with the to-be-aligned frame (*F*). The product is normalized and integrated, resulting in a CCV at each position. The position of the maximum CCV value found defines the corrected frame origin. Subsequently, the corresponding area in frame 2 is used as reference to align frame 3 again through cross-correlation comparison, and so on. Alternatively, an average of the rough aligned movie stack can be used as reference for the alignment of all frames. The cross-correlation method results in a list of fine alignment *X*- and *Y*-direction compensation values for each frame (*n*) (Figure 3C, traces labeled "fine align"). Applying the drift compensation values (Figure 3C) on a raw data movie, a drift corrected movie $X_{(\mathrm{corr})}Y_{(\mathrm{corr})}T$ stack (Figure 3D, individual $X_{(\mathrm{corr})}Y_{(\mathrm{corr})}$ frame 36) is generated. The corresponding kymograph $X_{(\mathrm{corr})}TY_{(\mathrm{corr})}$ stack (Figure 3E, individual $X_{(\mathrm{corr})}T$ frame containing all lines 75) nicely illustrates the drift correction of the frames and the stabilization of the molecule profiles that now appear as vertical stripes, as expected.

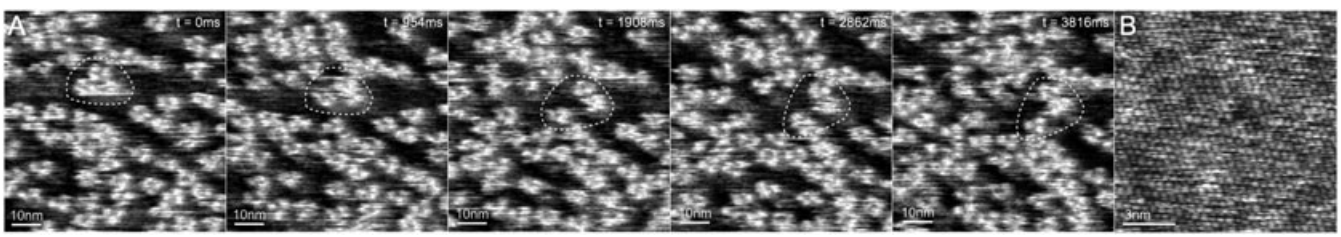


**Figure 2**. Drift and stability of the piezo-scanner and molecular movements. (A) Image sequence of the first 3816 ms of a longer HS-AFM movie. HS-AFM was performed in oscillating mode. Every second frame is shown spaced by 954 ms image acquisition time (full image size, 750 Å and 300 pixels square; sampling, 2.5 Å/pixel; original frame rate, 477 ms). Outline: assembly of three OmpF trimers that shift as a function of frame acquisition time from the left top to the right bottom. The trimers themselves present molecular movement with respect to each other. (B) High-resolution HS-AFM image (contact mode; frame rate, 2000 ms) displaying the crystalline arrangement of mica atoms with lattice constants of $a = b = 5.4$ Å; $\gamma = 60^\circ$, proving the high positional precision and stability of the piezo-scanner held at constant voltage over long time periods.



  

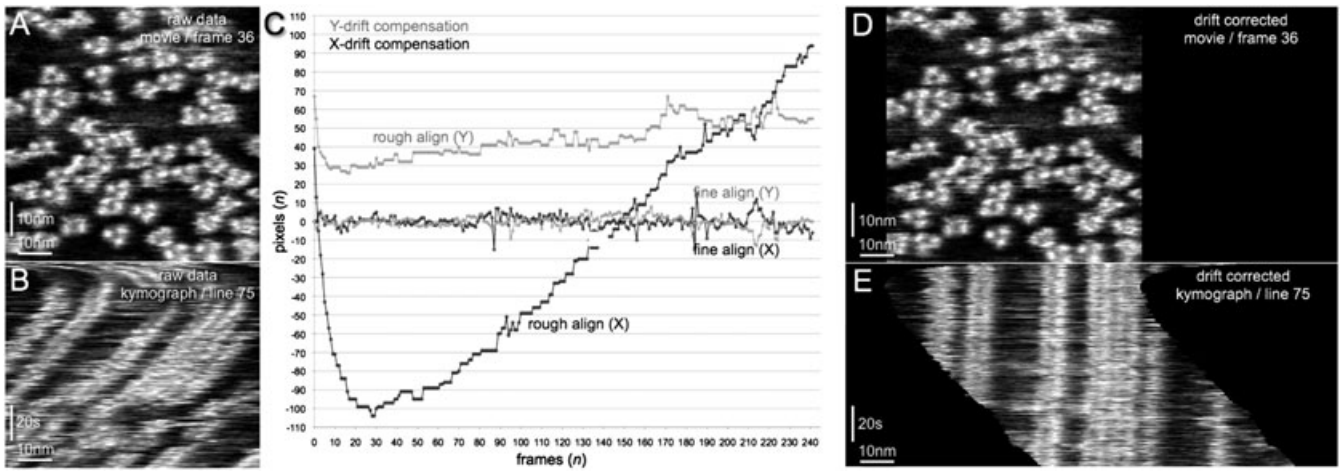


**Figure 3**. HS-AFM movie drift correction strategy. (A) Raw data frame (full image size, 750 Å and 300 pixels square; sampling, 2.5 Å/pixel) of the original *XYT* stack movie. (B) Frame of scan lines 75 of the *XTY*-kymograph stack. (C) Graph illustrating the *X* (black lines) and *Y* (gray lines) compensation values necessary for compensating the scanner drift during movie acquisition. The procedure comprises a manual rough align (if necessary) and a cross-correlation-based fine align step of the frames. (D) Frame 36 in the drift corrected $X_{(corr)}Y_{(corr)}T$ stack. (E) Frame of lines 75 of the $X_{(corr)}TY_{(corr)}$-kymograph stack assembled from the drift corrected movie.

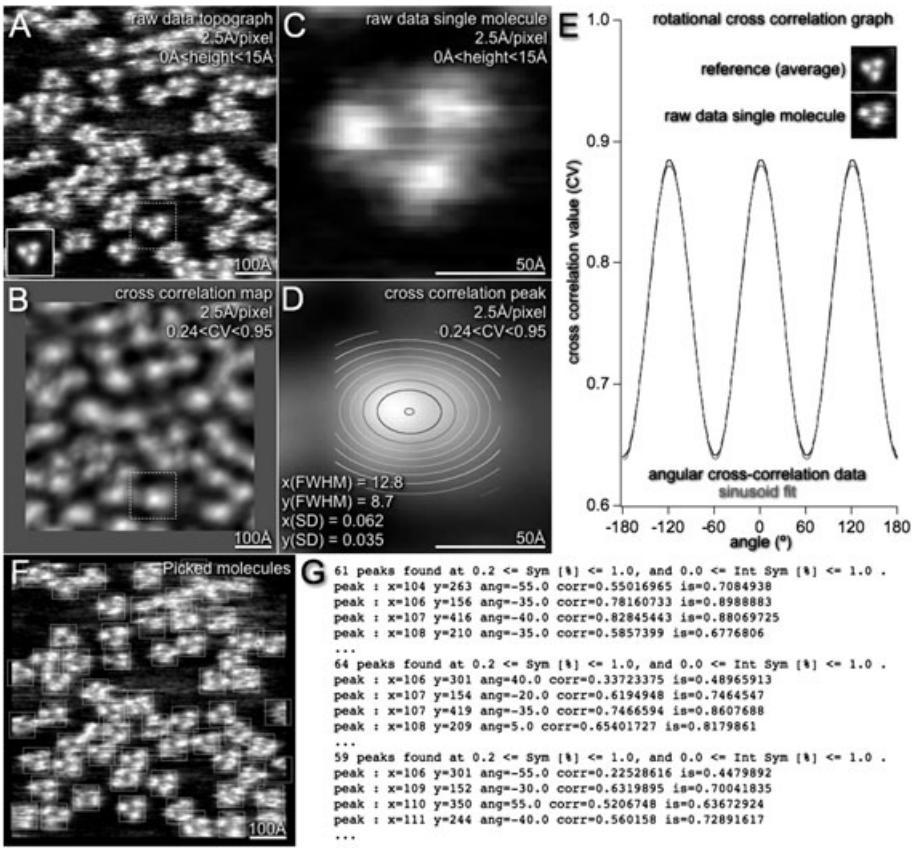


**Figure 4**. Definition of the lateral and angular position of molecules in HS-AFM images. (A) Raw data image (full image size, 750 Å and 300 pixels square; sampling, 2.5 Å/pixel). Inset: ensemble average used as reference for cross-correlation search. (B) Cross-correlation map of raw data image shown in panel A and the reference molecule shown in the inset in panel A (image dimensions are identical to panel A; full black to white scale $0.24 < CV < 0.95$, where a CV of 1 is identity). (C) Single molecule OmpF trimer outlined by dashed box in panel A. The panel shows the original pixel sampling. (D) Single cross-correlation peak outlined by dashed box in panel B, corresponding to the molecule shown in panel C overlaid by the 2-D Gaussian fit. The full-width at half-maximum values are 12.8 pixels and 8.7 pixels in *X*- and *Y*-dimensions, respectively, corresponding to 32 and 22 Å, respectively. The center of the molecules can be defined by the 2-D Gaussian fit to 0.062 pixel and 0.035 pixel (SD between CCV peak and 2-D Gaussian fit) along the *X*- and *Y*-axes, respectively, corresponding to 0.15 and 0.08 Å, respectively. (E) Graph displaying the CV between the average reference (top inset) and a single molecule (bottom inset) as a function of the rotation angle. The graph shows three maxima over 360° corresponding to the trimeric structure of OmpF. The sinusoid fit is superposed. The angular correlation maximum can be defined by the sinusoid fit to 3.5° (SD between angular CCV and sinusoid fit).

### Localization and orientation analysis of molecules

For all following analysis concerning molecular motion and interaction, at a first stage for each molecule the degrees of freedom, position *x*,*y*, and rotation angle $\alpha$ in each frame recorded at time *t* must be defined (Fechner *et al*., 2009). For this, each image frame (Figure 4A) is cross correlated with an ensemble average as reference (Figure 4A, inset). The resulting cross-correlation map (Figure 4B) reports peaks at positions where molecules are located (Figures 4A and 4B, dashed outline). The CCVs in this map range from 0.24 to 0.95, indicating the high-quality factor (3.95) of molecular localization definition above background. Single molecules are well resolved in raw data images at an original pixel sampling of 2.5 Å (Figure 4C). The CV peak of such a single molecule at that pixel sampling can be fitted by a two-dimensional (2-D) Gaussian fit defining the molecular position (*x*,*y*) with 0.1 Å precision (SD between peak CV values and fit) (Figure 4D). Given that the trimer structure of the molecule is well resolved (Figure 4C), the angular orientation ($\alpha$) of each molecule with respect to the reference can be unambiguously determined (Figure 4E). The CV shows angular dependence ranging from 0.89, when subunits of reference and molecule are in register, to 0.64, when subunits are misaligned (Figure 4E). The quality factor (1.39) suffices to let converge a fit of the angular CV graph with a precision (SD between angular CV trace and fit) of 3.5°. This way, all molecules in each image frame (Figure 4F) are characterized by their position (*x*,*y*), their angular orientation ($\alpha$), their CCV with respect to the reference, and additionally their IS, a value calculated from comparing a single molecule to itself after symmetrization, which we have found to be an adequate measure for the quality of a molecule (Fechner *et al*., 2009). These five values (*x*, *y*, $\alpha$, CV, IS) are further used for molecule diffusion and interaction analysis (Figure 4G).

### Two-dimensional diffusion analysis

In the experimental movie data, after contrast and drift correction (Figures 1–3), dynamics of molecules as a function of time are observed (Casuso *et al*., 2012). The cross-correlation-based determination of molecular positions (Figure 4) can now be exploited for diffusion analysis. For this, the molecular positions must be associated throughout the movie stack (i.e. time *T*) to construct molecular trajectories. The method used in the tracking is adapted from fluorescence microscopy single molecule tracking and based on simulated annealing (Racine *et al*., 2006), implemented and adapted in the software package. The input is the list of peaks (*x*, *y*, $\alpha$, CV, IS; Figure 4G) resulting from the particle picking analysis procedure. The tracking procedure involves an algorithm that aims to find the best association between the peaks based on their distance and by minimizing the corresponding overall energy function for connecting all peaks in the entire movie. The tracking procedure considers all the particles in frame (*n*) and linking them to all particles in frames ($n-1$) and ($n+1$) to define the object tracks. Because of imperfection of cross-correlation detection and drifting of molecules out of the observation field, a disappearance of molecules over a few consecutive frames is allowed. The resulting trajectory plots of the various molecules are overlaid to the movie frames for visualization (Figure 5). In this particular case (Casuso *et al*., 2012), we can see static molecules (outline 1) and mobile molecules (outline 2). The tracking results attribute a tag to each molecule to recover the trajectory and to compute statistics such as their root mean square displacement and their instantaneous speed. These data can be used for further analysis, such as the time-dependent diffusion coefficient of each molecule (Casuso *et al*., 2012).

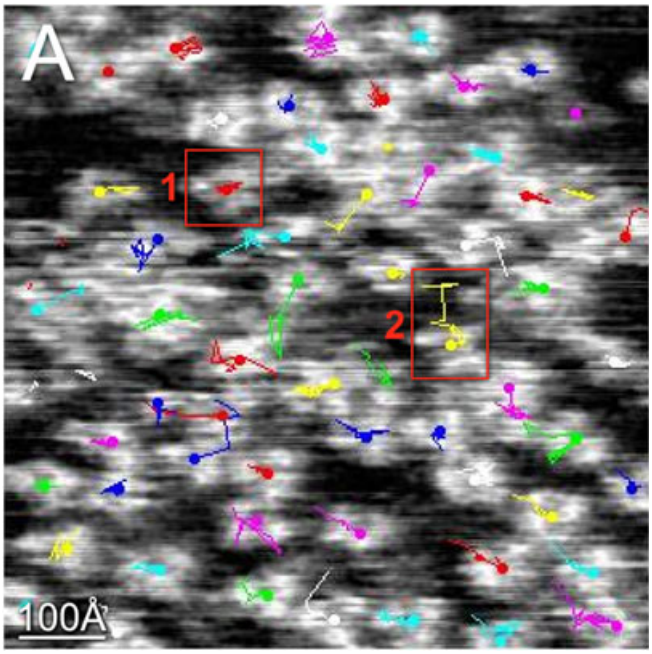


**Figure 5**. Molecule tracking. (A) Raw data image (full image size, 750 Å and 300 pixels square; sampling, 2.5 Å/pixel) frame (full movie length, 242 frames; 115434 ms; frame rate, 477 ms). The tracking traces are overlaid to the movie frames. Static (outline 1) and mobile molecules (outline 2) are found.

## DISCUSSION AND CONCLUSION

In this work, we present an HS-AFM movie analysis software that (i) adjusts the image contrast line by line and filters noise (Figure 1), (ii) corrects for mechanical and piezo-scanner drift (Figures 2 and 3), (iii) analyzes the molecular particle localization and angular orientation (Figure 4), and (iv) performs particle tracking and derives the molecular motion parameters (Figure 5).

This work flow is motivated by the following: (i) improved contrast and image de-noising will aid all further data treatment and visualization, (ii) real space superposition molecular motion can be precisely analyzed and visualized only in movies with perfect frame, and (iii) determination of the degrees of freedom of a molecule allows (iv) the detailed analysis of molecule tracking and protein interaction profiles and the determination of dynamic parameters such as the root mean square displacement of single molecules.

This analysis software has improved the visibility of data and rendered possible the detailed analysis of approximately 15 000 molecule images (~60 molecules in ~250 movie frames) concerning their localization, angular orientation, and dynamic properties (Casuso *et al*., 2012).

This AFM-devoted software package is inspired by both electron microscopy and optical microscopy image treatment and analysis procedures. The part that uses cross-correlation-based searches to define molecular localization and orientation and that averages molecules is strongly reminiscent to procedures used in electron microscopy 2-D crystal and single



  

particle analysis (Frank *et al*., 1987; Saxton *et al*., 1979). The part that concerns molecule tracking and dynamics analysis is adapted from optical microscopy single particle tracking where the point spread function of a fluorescence signal is detected and analyzed (Racine *et al*., 2006; Marguet *et al*., 2006). These procedures are preceded by an AFM-specific line-by-line data treatment that compensates for apparatus specific imprecision and noise.

We believe that HS-AFM is unique in its capabilities to monitor structure and dynamics at the single molecule level (Casuso *et al*., 2012; Casuso *et al*., 2010; Kodera *et al*., 2010; Shibata *et al*., 2010) and will open novel fields of investigation. With the software development presented here, we aim at providing a solid platform for data treatment and analysis to base future investigation on solid ground and to provide high credibility to presented studies of HS-AFM.

## REFERENCES

Ando T, Uchihashi T, Kodera N, Yamamoto D, Taniguch M, Miyagi A, Yamashita H. 2008. Invited Review: High-speed AFM and nano-visualization of biomolecular processes. *Europ. J. Physiol* **456**: 211–225.

Ando T, Kodera N, Takai E, Maruyama D, Saito K, Toda A. 2001. A high-speed atomic force microscope for studying biological macromolecules. *Proc. Natl. Acad. Sci.* **98**(22): 12468–12472.

Binnig G, Quate CF, Gerber C. 1986. Atomic Force Microscope. *Phys. Rev. Lett.* **56**(9): 930.

Casuso I, Khao J, Chami M, Paul-Gilloteaux P, Husain M, Duneau JP, Stahlberg H, Sturgis J, Scheuring S. 2012. Membrane interaction pathway and potential map of a membrane protein by high-speed atomic force microscopy. *Journal: under review*.

Casuso I, Sens P, Rico F, Scheuring S. 2010. Experimental Evidence for Membrane-Mediated Protein-Protein Interaction. *Biophys. J.* **99**(7): L47–L49.

Casuso I, Scheuring S. 2010. Automated setpoint adjustment for biological contact mode atomic force microscopy imaging. *Nanotechnology* **21**(3): 35104–35111.

Chen S-W, Pellequer J-L. 2011. DeStripe: frequency-based algorithm for removing stripe noises from AFM images. *BMC Struct. Biol.* **11**(1): 7.

de Pablo PJ, Colchero J, Gomez-Herrero J, Baro AM. 1998. Jumping mode scanning force microscopy. *Appl. Phys. Lett.* **73**(22): 3300–3302.

Engel A, Gaub HE. 2008. Structure and Mechanics of Membrane Proteins. *Annu. Rev. Biochem.* **77**(1): 127–148.

Fantner GE, Schitter G, Kindt JH, Ivanov T, Ivanova K, Patel R, Holten-Andersen N, Adams J, Thurner PJ, Rangelow IW, Hansma PK. 2006. Components for high speed atomic force microscopy. *Ultramicroscopy* **106**(8–9): 881–887.

Fechner P, Boudier T, Mangenot S, Jaroslawski S, Sturgis JN, Scheuring S. 2009. Structural Information, Resolution, and Noise in High-Resolution Atomic Force Microscopy Topographs. *Biophys. J.* **96**(9): 3822–3831.

Frank J, Bretaudiere J-P, Carazo J-M, Veschoor A, Wagenknecht T. 1987. Classification of images of biomolecular assemblies: A study of ribosomes and ribosomal subunits of *Escheria coli*. *J. Microsc.* **150**:99–115.

Kindt JH, Thompson JB, Viani MB, Hansma PK. 2002. Atomic force microscope detector drift compensation by correlation of similar traces acquired at different setpoints. *Rev. Sci. Instrum.* **73**(6): 2305–2307.

Kodera N, Yamamoto D, Ishikawa R, Ando T. 2010. Video imaging of walking myosin V by high-speed atomic force microscopy. *Nature* **468**(7320): 72–76.

Kusumi A, Sako Y, Yamamoto M. 1993. Confined lateral diffusion of membrane receptors as studied by single particle tracking (nanovid microscopy). Effects of calcium-induced differentiation in cultured epithelial cells. . *Biophysical Journal* **65**: 2021–2040.

Marguet D, Lenne PF, Rigneault H, He HT. 2006. Dynamics in the plasma membrane: how to combine fluidity and order. *EMBO J.* **25**: 3446–3457.

Parot P, Dufrêne YF, Hinterdorfer P, Le Grimellec C, Navajas D, Pellequer J-L, Scheuring S. 2007. Past, present and future of atomic force microscopy in life sciences and medicine. *J. Mol. Recognit.* **20**(6): 418–431.

Racine V, Hertzog A, Jouanneau J, Salamero J, Kervrann C, Sibarita JB. 2006. Multiple-target tracking of 3D fluorescent objects based on simulated annealing. 2006 3rd Ieee International Symposium on Biomedical Imaging: Macro to Nano, Vols **1–3**, New York: IEEE. p 1020–1023.

Rasband WS. 1997–2011. ImageJ. *Rasband, W.S., ImageJ, U. S. National Institutes of Health, Bethesda, Maryland, USA*, http://rsbweb.nih.gov/ij/.

Rico F, Roca-Cusachs P, Gavara Nr, FarrÈ R, Rotger M, Navajas D. 2005. Probing mechanical properties of living cells by atomic force microscopy with blunted pyramidal cantilever tips. *Physical Review E* **72**(2): 021914.

Rief M, Gautel M, Oesterhelt F, Fernandez JM, Gaub HE. 1997. Reversible unfolding of individual titin immunoglobulin domains by AFM. *Science* **276**(5315): 1109–12.

Saxton WO, Pitt TJ, Horner M. 1979. Digital image processing: The semper system. *Ultramicroscopy* **4**: 343–354.

Schabert FA, Engel A. 1994. Reproducible acquisition of *Escherichia coli* porin surface topographs by atomic force microscopy. *Biophys. J.* **67**(6): 2394–2403.

Schabert FA, Henn C, Engel A. 1995. Native Escherichia coli OmpF porin surfaces probed by atomic force microscopy. *Science* **268** (5207): 92–94.

Shibata M, Yamashita H, Uchihashi T, Kandori H, Ando T. 2010. High-speed atomic force microscopy shows dynamic molecular processes in photoactivated bacteriorhodopsin. *Nat. Nanotechnol.* **5**(3): 208–212.

Thomson NH, Fritz M, Radmacher M, Cleveland JP, Schmidt CF, Hansma PK. 1996. Protein tracking and detection of protein motion using atomic force microscopy. *Biophys. J.* **70**(5): 2421–2431.

Unser M, Trus BL, Steven AC. 1987. A new resolution criterion based on spectral signal-to-noise ratios. *Ultramicroscopy* **23**(1): 39–51.

van Noort SJT, van der Werf KO, de Grooth BG, Greve J. 1999. High Speed Atomic Force Microscopy of Biomolecules by Image Tracking. *Biophys. J.* **77**(4): 2295–2303.

VanCleef M, Holt SA, Watson GS, Myhra S. 1996. Polystyrene spheres on mica substrates: AFM calibration, tip parameters and scan artefacts. *J. Microscopy-Oxford* **181**: 2–9.

Viani MB, Pietrasanta LI, Thompson JB, Chand A, Gebeshuber IC, Kindt JH, Richter M, Hansma HG, Hansma PK. 2000. Probing protein-protein interactions in real time. *Nat. Struct. Mol. Biol.* **7**(8): 644–647.

Viani MB, Schaffer TE, Paloczi GT, Pietrasanta LI, Smith BL, Thompson JB, Richter M, Rief M, Gaub HE, Plaxco KW, Cleland AN, Hansma HG, Hansma PK. 1999. Fast imaging and fast force spectroscopy of single biopolymers with a new atomic force microscope designed for small cantilevers. *Rev. Sci. Instrum.* **70**(11): 4300–4303.